Development and validation of a numerical tool for the simulation of the temperature field and infrared radiance rendering in an urban scene

by N. Lalanne*, J-C. Krapez*, C. Le Niliot**, X. Briottet***, J. Pierro* and L. Labarre****

* ONERA-SALON, BA 701, 13661 Salon cedex air, France, *nicolas.lalanne @, krapez@, pierro @onera.fr*
** IUSTI, 13453 Marseille cedex 13, France, *christophe.leniliot @univ-amu.fr*
*** ONERA-TOULOUSE, 31055 Toulouse cedex 4, France, *xavier.briottet @onera.fr*
**** ONERA-PALAISEAU, 91123 Palaiseau cedex, France, *luc.labarre @onera.fr*

Abstract

We present a numerical tool aimed at simulating infrared images of an urban environment, by solving the direct heat transfer problem, and then computing the radiance rendering at the sensor level. SOLENE (Cerma, Nantes) was coupled with two software packages developed at ONERA: SUSHI (Simulation in Urban Scene of Heat dIffusion) and MOHICANS (MOdélisation Hyperspectrale d'Images en entrée Capteur pour l'ANalyse et l'inversion du Signal) for realizing this task. SUSHI is also used for computing the surface temperatures: either a 1D model or a 2D model is used. We present the whole software chain, its validation by software and experimental analysis.

1. Introduction

Human activity in the urban context influences the local environment. For instance a practical consequence in terms of urban climatology is the development of urban heat islands. The urban climate is the result of thermal and water flow processes between the urban surfaces and the environment. Infrared remote sensing is a powerful tool for measuring the influence of these interactions on the urban surfaces at different spatial scales. The infrared images obtained with airborne sensor inform about the thermal balance of urban components and, at a large scale, about the urban heat island. The radiance images are however a complex result of various influences both on the thermal level and on the radiative level; therefore a theoretical model is often necessary for interpreting these images. This model should first take into account the energy budgets for the different surfaces (roofs, roads, walls, etc.) including the radiative interactions between them. It should then solve the heat transfer problem through the solid materials of the urban scene at a scale compatible with the sensor resolution, which can be of the order of a tenth of a meter. The computed surface temperature field has finally to be combined with the emissivity field in a radiative transfer module for getting the at-sensor infrared radiance image. The energy exchanges between cities and the atmosphere can be simulated at a scale between the mesoscale (whole city) and the building scale; such models as for example TEB [1] and SM2-U [2]. A second category of models includes the thermo-radiative models establishing the energy budget at a scale significantly lower than the building size (typically one meter or less). These models estimate all terms of the energy budget, in order to compute the temperature. A list of such models is described in table 1.

Table 1. *Main existing thermo-radiative urban models*

Model : autors, (NAME), year	Groleau et al. SOLENE [9] (2003)	Krayenhoff, Voogt TUF-3D [6] (2007)	Asawa, Hoyano [5] (2008)	Kastendeuch, Najjar [4] (2008)	Yang, Li MUST [8] (2013)
3D scene	From SketchUp	3D cells organized in cluster geometry	3D-CAD with trees		3D cells organized in cluster geometry
Direct solar	Measure or Perrin de Brinchambault model	Iqbal (83)	Bouguer's law	Measure + position by Reda Afshin	Bouguer's law
Diffuse solar	Measure + "all weather" Perez sky	Iqbal (83)	Nagata's formula	Measure + "all weather" Perez sky	Berlage's relation
Atmospheric radiation	Measure + sky view factor	Prata (96)	Brunt's formula	Measure + homogeneous	Model of Berdahl and Martin (84)
Shape factor	By subdivision in triangular facets	Exact plane parallel analytical equation	Deduced from sky view factor	Pianykh (98)	By a method similar to Monte Carlo
Multiple reflections VNIR	Progressive refinement	Two reflections minimum	One	Progressive refinement	Gebhart factor
Multiple reflections IR	Progressive refinement (not with sky)	Isotropique sky radiance	CN + other surface at T_{air}	Progressive refinement (not with sky)	Gebhart factor
Sensible heat flow	Imposed h	Function of surface roughness and effective wind speed	Jürges's formula	h by Ito (78)	Function of surface roughness and effective wind speed
Wall thermal model	Nodal (5)	Finite differences + iterative process with IR radiation	Finite differences (5 days)	Finite differences + iterative process with IR radiation	Finite differences
Main limitation	Limited number of nodes	Simplified geometry (3D Cartesian)	Simplified reflection of VNIR & IR fluxes	Wall discretization	Simplified geometry (3D Cartesian)

The thermo-radiative model SOLENE [9], developed at CERMA Nantes, solves the heat conduction problem in walls with a nodal method based on a preliminary evaluation of the radiative heat fluxes on the boundaries. This 5 nodes model can describe a wall with only one or two layers. The simplicity of this model does not correctly capture the behavior of complex walls, heavy inertial materials, or semi-infinite ground [10]. The radiative exchanges between the surfaces and the sky are computed from the view factors and an approximate radiosity method, partly based on an iterative algorithm named "progressive refinement". In the IR domain, a blackbody assumption is used for computing the radiative heat exchanges between surfaces. Experimental validations have shown that this model can induce deviations between the simulated and the measured heat fluxes, and thereafter between the simulated and measured temperatures [11].

[12] identify three general classes of methods for solving the heat conduction equation: numerical methods, response factor (RF) methods and conduction transfer function (CTF) methods [13]. Numerical methods correspond to methods discretizing the studied domain in meshes, and where the solutions of the differential equations are approximated by numerical techniques as FDM, FVM, FEM, etc. The RF method is based on the responses of the thermal system to an elementary stress and they are convoluted by the observed thermal excitations. The CTF takes further into account previous values of the searched variable. These methods are based on the Laplace transformation and are commonly used in building energy software packages. For instance, the RF method is adopted by DOE-2 whereas the CTF method is found in EnergyPlus or TRNSYS. Both methods are used for computing the wall heat flux density from the outside and inside temperatures (actually the outside sol-air temperature and the inside air temperature) which actually can be considered as an inverse problem. However the main unknown variable for simulating an infrared image of a given urban scene is not the wall heat flux density but the building external temperature, therefore we developed our own thermal model called SUSHI (Simulation in Urban Scene of Heat dIffusion).

It is linked to SOLENE from which it gets some radiative parameters for evaluating the radiative energy budget like the sky model, the view factor matrix and the net radiative flux in the solar spectrum. SUSHI solves the heat equation for wall elements where the heat conduction is either 1D or 2D. The purpose is to simulate extended areas where heat flows normally to the surface and localized areas, generally associated to thermal bridges, where the heat flow is 2D, as for L-shapes (building corners) and T-shapes (wall/floor junction).

Once the temperature field is known, the radiance images at sensor level can be realized. A radiative transfer code is required to take into account the photonic interactions in the scene. The atmospheric radiative transfer codes are based on the radiative transfer equation and can calculate spectral characteristics of the atmosphere along the line of sight (transmission, self-emission, molecular scattering …). They are limited to simplified geometry (plane or spherical ground). 3D radiative transfer codes were thus developed in order to take into account radiative interactions between 3D elements of the scene. In the infrared domain, such codes are DART [14] and TITAN [15]. Main limits DART are in the spatial resolution of its thermal model. On the other hand TITAN computes radiative transfers with a high spatial resolution, but it has no thermal model. Thereafter, we use the new radiative transfer code MOHICANS which is a combination of AMARTIS [22] and TITAN. The interest of this code is to simulate a hyperspectral sensor in [0.4 – 14 µm].

In the following we will describe the main aspects of the thermal code SUSHI and its coupling with SOLENE and MOHICANS. Then we will present the results of various validation steps, in particular the comparison with experimental results obtained during the BATIR 2013 measurement campaign where infrared thermography of two buildings was performed with two ground cameras and an airborne camera.

2. Models

2.1. Outline

In order to obtain a simulated spectral image of an urban scene in the thermal IR spectral domain [3-15 µm], the temperature field over all external surfaces has to be computed. For this purpose, the heat equation describing the thermal transfer through the walls, roofs and soil has to be solved. The high spatial resolution of present IR cameras requires considering surface elements of area less than one square meter. Depending on their location on the wall, the heat transfer through these elements can be considered as one dimensional or not. Generally speaking, 2D transfer is observed at each corner of the building envelope (L-shape), and at thermal bridges like the floor/wall junctions (T-shape). 3D transfer is observed for example at a corner of a floor/wall junction. Finally, 1D transfer is observed over the building envelope far from previous thermal singularities. The numerical tool we developed allows simulating the thermal behaviour of walls presenting areas where heat flow is one of these two types: 1D or 2D. It takes into account the atmospheric conditions as measured with a series of meteorological sensors. It also takes into account the building internal conditions as recorded with temperature sensors. These external/internal conditions are recorded for a sufficiently long period of time for allowing a dynamic thermal analysis prone to capture all thermal inertia effects.

A series of programs are used as described in the chart in figure 1:
- SketchUp is used to build-up the 3D-scene and subdivide each wall in areas where heat flow is either 1D or 2D;
- SOLENE software which was developed at CERMA laboratory is used for meshing each area, for computing the view factors and then the solar radiation energy budget after multiple reflections modelling and shadow tracing at each time step;
- SUSHI thermal software (Simulation in Urban Scene of Heat dIffusion) is used for modeling the infrared radiation energy budget, the heat convection flux and then for solving the 1D and 2D heat transfer problems inside the wall and soil elements.

- MOHICANS is finally used to get the spectral infrared radiance reaching each element of the sensor matrix from the temperature field computed by SUSHI and from the atmosphere radiative parameters computed by MATISSE [16].

SketchUp	SOLENE	SUSHI	MOHICANS	MATISSE
3D scene	Solar net flux density	Temperature field	Radiance at sensor level	Atmospheric terms
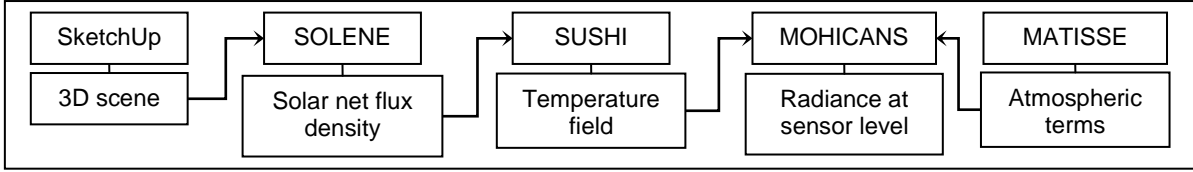
Fig. 1. Flow chart of programs used in the full simulation

2.2. Thermal model: SUSHI

2.2.1. Time evolution

Temperature and fluxes are assumed to be periodic. This allows applying the Fourier transform which, thanks to the Fast Fourier Transform tool, leads to semi-analytical solutions and yields the results in a very short time. However, for the input, we have to consider real meteorological data and these data are in part stochastic. The question was then how to choose the period aimed at representing the periodical phenomena. Of course it should be 24h at least. If it is too short, let us say only 24h, the computed temperature would be in error due to fact that the atmospheric conditions were actually different during any day before. One should thus extend the duration of the period. In this way, the first mismatch between the modelled atmospheric conditions (i.e. through the periodicity assumption) and the real atmospheric conditions would be rejected further back in the past. The error on the computed temperature would then be lowered at the expense of a longer computing time. The optimal choice for the period duration will be discussed in § 3.1.

2.2.2. Boundary conditions

Elements of mesh can exchange energetic fluxes with the environment. In the general case, these fluxes are convective and radiative. The radiative fluxes are subdivided into solar and infrared components. One supposes that solar radiation can be absorbed or reflected by a surface, and that infrared components can be absorbed, reflected and reradiated to others surfaces. The solar radiation may also be split into a direct and a diffuse component, in order to give hourly shadow distribution. The software SOLENE is used to compute these solar components. In this software, the direct component follows the Perrin de Brinchambault formula, and the atmospheric diffuse component follows the "all weather model for sky luminance" of Perez et al. [17]. This provides spectral-integrated fluxes depending on place and hour, and on sky clearness and brightness for the diffuse component. The energy budget through multiple reflections is computed by the progressive refinement radiosity method [18] which first requires the calculation of the view factors between all surfaces of the scene including the "sky facets". SOLENE however doesn't apply the progressive refinement radiosity method for evaluating the infrared radiative net fluxes, it rather considers a blackbody assumption. For avoiding this approximation we chose to perform a more rigorous infrared radiative exchange calculation by implementing the same progressive refinement radiosity method as in the visible.

Let us now consider the convective flux on the outdoor building surface. It may be modelled through a convective coefficient which depends on wind velocity and orientation, on air temperature, on local and global geometry, etc. Using a 3D fluid mechanics solver provides a precise modelling for this coefficient [23]. However, for keeping a reasonable computational time, we preferred to use one among several empirical formulas giving the convective coefficient vs. wind velocity in the building thermal energy context; the coefficient is thus time dependant: $h(t)$.

The thermal balance at the outdoor building surface can be expressed as follows:

$$-\lambda \frac{\partial T_i}{\partial z} = -h(t)\left(T_i - T_a(t)\right) - R_{vis}^{net}(t) - R_{IR}^{net}\left(t, T_i, T_{j \neq i}\right)$$ (1)

It can be considered as a second order boundary condition where the specified heat flux corresponds to the right-hand side of the equation. T_a is air temperature, R_{vis}^{net} is the net radiative flux in the visible domain and R_{IR}^{net} is the net radiative flux in the infrared domain; it depends on the atmospheric IR radiation, on the temperature of the surface of interest and on the temperature of the surfaces exchanging radiation with it. This dependence on temperature is nonlinear which requires solving the problem through iterations. The time dependence of $h(t)$ would also require iterations even though an alternative exists which avoids performing iterations but requires more involved algebra [24].

For speeding up the iteration process, the second order boundary condition can be replaced by the following third order boundary condition with a *constant* arbitrary coefficient h^{fict}:

$$-\lambda \frac{\partial T_i}{\partial z} = -h^{fict}\left(T_i - T_{sa}(t)\right)$$ (2)

where $T_{sa}(t)$ corresponds to a modified sol-air temperature which is defined by:

$$T_{sa}(t) = T_i - \frac{1}{h^{fict}}\left[h(t)(T_i - T_a(t)) + R_{vis}^{net}(t) + R_{IR}^{net}(t, T_i, T_{j \neq i})\right] \tag{3}$$

In other words, the thermal excitation associated with the 3rd order BC is:

$$\left(h^{fict} - h(t)\right)T_i + h(t)T_a(t) - R_{vis}^{net}(t) - R_{IR}^{net}(t, T_i, T_{j \neq i}) \tag{4}$$

A first iterative process identified by (1) in figure 2 is implemented by updating only the convective flux term $\left(h^{fict} - h(t)\right)T_i$. When the convergence criterion is reached, the radiative flux term $R_{IR}^{net}(t, T_i, T_{j \neq i})$ is updated (step (2) in figure 2) and the global iterative process is repeated. The iterative process is split into two steps because updating the radiative flux terms is the most expensive. For the indoor boundary condition, it's assumed that the environment is homogeneous and characterised by the air temperature and by a global constant radiato-convective transfer coefficient.
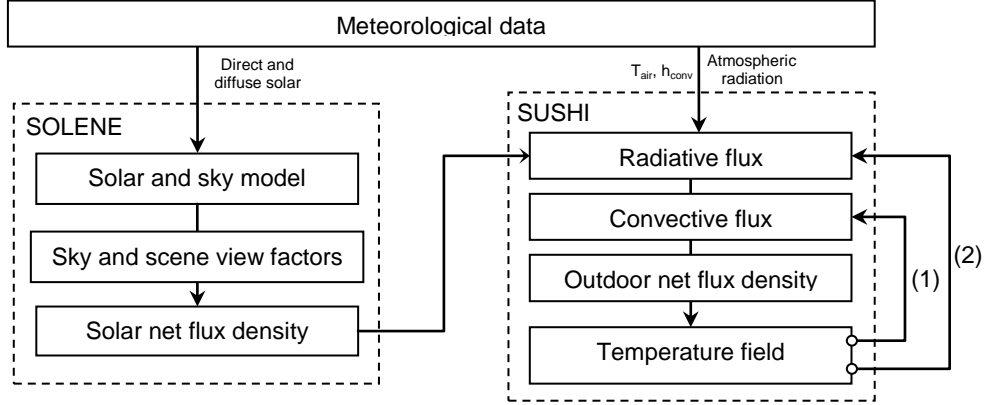
Fig. 2. *Flow diagram of the computed terms by SOLENE and SUSHI*

2.2.3. 1D configuration

As explained before, the 1D transfer model is used for those facets of wall that are far from thermal singularities like facade corners, wall/floor junctions, … . Its semi-infinite version is used for soils. The walls may be composed of many layers. It is assumed that each layer is homogeneous, isotropic with constant thermal properties. The thermal problem is solved by applying the quadrupole technique after performing a Fourier transform to the heat equation and to the boundary conditions [21]. The following backward transfer relation relates the temperatures and conduction heat flux at front and back sides of the wall:

$$\begin{pmatrix} \tilde{T}_e \\ \tilde{\varphi}_e \end{pmatrix} = \begin{pmatrix} A & B \\ C & D \end{pmatrix}\begin{pmatrix} \tilde{T}_s \\ \tilde{\varphi}_s \end{pmatrix} \tag{5}$$

where the tilde represents the Fourier transform of the corresponding variable, and where

$$\begin{pmatrix} A & B \\ C & D \end{pmatrix} = \prod_{i=1}^{N_{layers}}\begin{pmatrix} A_i & B_i \\ C_i & D_i \end{pmatrix} \tag{6}$$

is the total quadrupole matrix, which is calculated by multiplication of each quadrupole matrix, with A_i, B_i, C_i and D_i the quadrupole coefficients of the layer i. By isolating the front temperature it can be expressed by the indoor and outdoor exchanged net flux densities. The formulation of the terms of the quadrupole matrix proposed by [19] is used. The temperature expression is also written:

$$\tilde{T}_{ex} = X\,\tilde{Q}_{ex} + Z\,\tilde{Q}_{in} \tag{7}$$

with: $\quad X = \Lambda^{-1}\left(A' + h_{in}^g B'\right) \qquad\qquad$ the outdoor transfer function,

$\quad \tilde{Q}_{ex} = \tilde{\varphi}_{VNIR}^{abs} - \tilde{\varphi}_{IR}^{net^k} - TF(\Delta h_{ex}T_{ex}^{\ k}) + TF(h_{ex}T_{ex}^{air}) \qquad$ the outdoor net flux density,

$\quad Z = \Lambda^{-1}\exp\left(-\left[\sum_{i=1}^{N_{layers}}\xi_i\right]\sqrt{j\omega}\right) \qquad\qquad$ the indoor transfer function,

$\quad \tilde{Q}_{in} = -h_{in}^g \tilde{T}_{in}^{air} \qquad\qquad$ the indoor net flux density

and $\quad \Lambda = h_{ex}^{fict}A' + h_{ex}^{fict}h_{in}^g B' + C' + h_{in}^g D'$,

A', B', C' and D' are the reduced quadrupole coefficients (i.e. divided by the exponential of positive argument), h_{ex}^{fict} the fictive convective external coefficient, h_{in}^g the radiato-convective internal coefficient, φ_{VNIR}^{abs} the absorbed solar

flux, $\varphi_{IR}^{net^k}$ the net infrared flux computed by $T_{ex}^{\ k}$ the temperature calculated on previous iteration, h_{ex} and Δh_{ex} the convective external coefficient and his difference to the fictive convective coefficient, T_{ex}^{air} and T_{in}^{air} the external and internal air temperature, ξ_i the square root of time diffusion of the layer i, ω the pulsation and j the imaginary variable.

The temperature is obtained after an inverse Fourier transform of $\tilde{T}_{ex}$. The convective term $\Delta h_{ex} T_{ex}^{\ k}$ can then be updated for a next iteration. Periodically the radiative term $\tilde{\varphi}_{IR}^{net^k}$ is also updated as described in figure 2.

2.2.4. 2D configuration

When the one-dimensional assumption is no valid, as observed in the vicinity of thermal bridges, the transfer functions related to those facets are pre-calculated by the finite element method as provided by the CAST3M software. The objective is to get periodic transfer functions corresponding to the response of a thermal bridge when an elementary flux is applied over each one of the characteristic surfaces of the thermal bridge. Thus, when considering the symmetric L-shape at left of figure 3, a uniform flux is applied on S1, then on S3 (due to symmetry, the response is the same when the perturbation is applied on S1 or on S2). Similarly, for the symmetric T-shape at right of figure 3 a uniform flux is applied on S1, then on S2. In all cases, a unitary step heating is applied for a relatively long period of time, typically several days. The transient response of the system is subtracted to itself after moving it one time step for getting the response to an elementary pulse. This response is then added to itself after moving it 24h, then 48h, … N times for getting the periodic response to an elementary pulse (N should be sufficiently long for approaching the true periodic response). The Fourier transform of the periodic responses $\tilde{G}_l^p(x, \omega_k)$, $l = 1,3$ related to all external facets (facets on S1 and S2 for the L-shape and facets on S1 for the T-shape) are then stored for future computations of the external temperature according to:

$$\tilde{T}(x, \omega_k) = \sum_{l=1}^{3} \tilde{G}_l^p(x, \omega_k).\tilde{Q}_l(\omega_k) \tag{8}$$

where $\tilde{Q}_l(\omega_k)$ is the Fourier transform of the net heat flux density averaged over surface S_l and x is the position on the external surface with respect to the thermal bridge center. For returning into the temporal space an inverse fast Fourier transform is finally performed with the IFFTW algorithm [20].
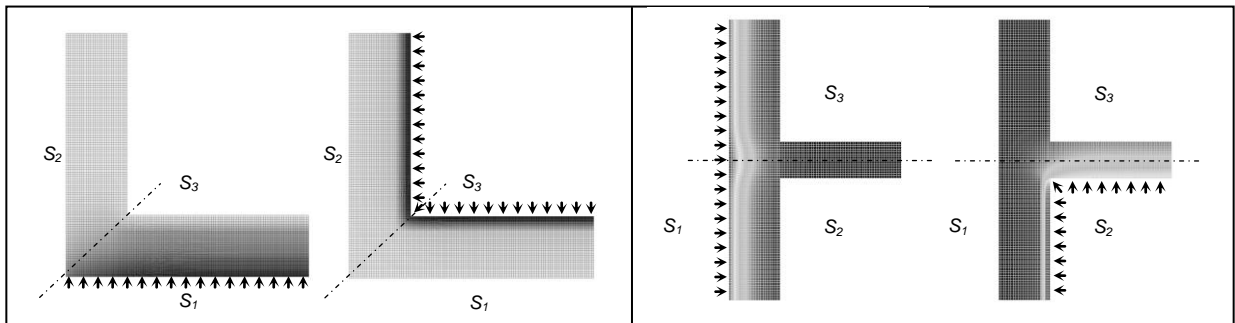
Fig. 3. Drawing of L-shape (at left) and T-shape (at right) (imposed flow located by arrows)

2.3. Spectral model: MOHICANS
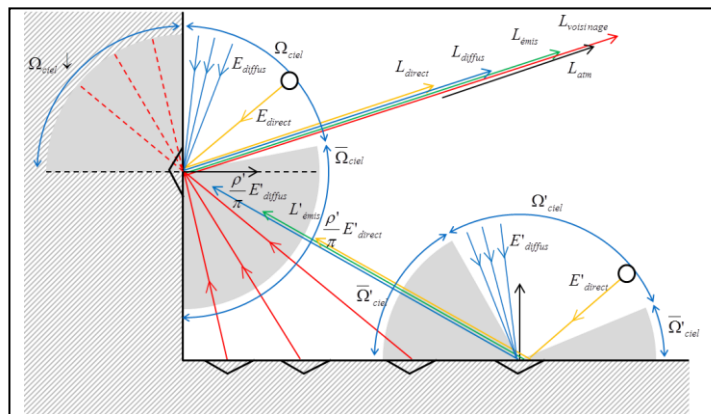
Fig. 4. Drawing of radiative terms computed by MOHICANS which contribute to the radiance at sensor level

The software MOHICANS is a numerical tool developed at ONERA which aims at evaluating all radiative components contributing to the optical signal received by a multi or hyperspectral sensor over a 3D scene. It is actually a fusion of previously developed codes AMARTIS [22] for the visible to near infrared range and TITAN [15] for the midwave to longwave infrared range. Both of them rely on atmospheric radiative computations by MATISSE [16]. The spectral domain finally covers the 0.4 to 15 μm range. MOHICANS is organized in four calculation steps: (i) computation of the sky irradiance hemisphere and the atmosphere transmission terms by calls to MATISSE, (ii) computation of geometrical terms corresponding to sun visibility, facet to facet visibility and facet to pixel visibility, (iii) computation of total irradiance, corresponding to the sum of solar direct irradiance, the atmosphere irradiance and the environment irradiance, (iv) computation of the radiance of the radiative flux reaching each pixel of the imaging sensor. A schematic of the radiative exchanges between two facets of a wall-soil angle is presented in figure 4.

3. Computation results

3.1. Temporal configuration

The first analysis concerns the validation of the time *periodic* model. For simulating the temperature field over a one day time interval $[t_0-24, t_0]$ we assume that the radiative and convective fluxes are periodic with a period D and that their variations are those observed during the time interval $[t_0-D, t_0]$ with $D=kx24; k\geq1$. The longer the period D, the lower the error on temperature over the interval $[t_0-24, t_0]$ due to the wrong assumption of periodic phenomena. The minimum number k of days to consider for getting an error lower than a specified value was determined by considering both an elementary part of a typical wall (see properties in table 2) and a semi-infinite ground (effusivity: $b=707\ SI$). Both were submitted to the real atmospheric fluxes observed during the BATIR campaign for a horizontal surface. A long period D of 12 days was considered as a reference. Temperature was computed for progressively shorter periods D and compared to this reference. The maximum difference and the RMS error value over the day of interest (i.e. the last one) are plotted in figure 3 for the wall and the ground). These simulations highlight that a period of two days is long enough for the wall (maximum error of 0.1°C; RMS<0.02°C), but that a period of five days is necessary for soils, when setting the maximum error criterion to 0.1°C. Anyway, with a period of two days, the maximum error on temperature for the soil is not more than about 0.2°C. For the remaining we will thus perform the thermal simulations with $D=48h$.
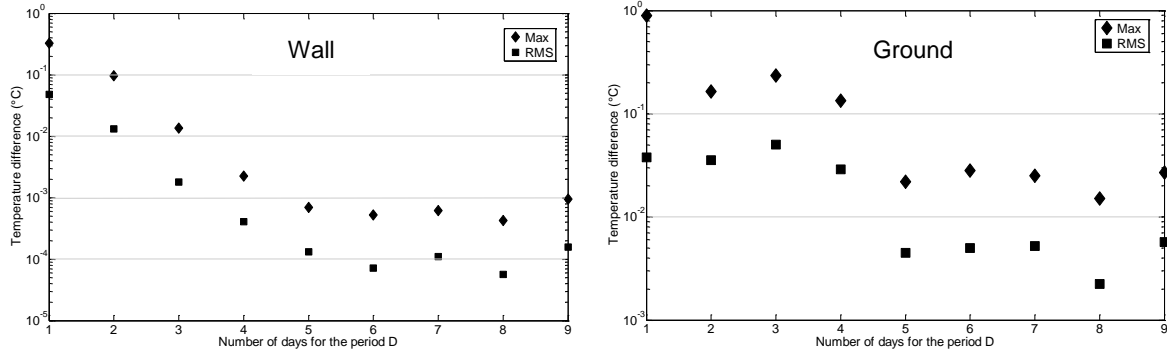
Fig. 5. *RMS and absolute maximal difference temperature according to the number of considered periods for a wall (left) and a ground (right)*

3.2. Sensitivity study

A MATLAB program which calculates surface temperature in the very same manner as the 1D SUSHI model is used for local and fast simulations. Analytical validations of the quadrupole model were performed on basic configurations like a semi-infinite layer with or without convective losses, with a sinusoidal imposed boundary flux. Software validations on finite walls were then realized by means of comparison with SOLENE simulations. In the case of a single horizontal two layer slab (with an isolating layer), both models give similar results. However, SUSHI results are much closer to the analytical solution as compared to SOLENE results for very thick materials and for soils. In addition, SUSHI permits to model walls with more than two materials.

In a second phase, the sensitivities of the front temperature with respect to thermal, convective and radiative parameters are analysed. area series of 14 parameters were analyzed: the effusivity and the square root of the diffusion time each of the three layers of the wall (see table 2), the albedo and the emissivity of the external surface, the external and internal convective coefficients, the external and internal air temperature, and the VNIR (Visible and Near Infrared, i.e. solar spectrum) and IR incident flux density.

We define two groups of parameters, according to their time dependency. The external convective coefficient, the air external and internal temperature and the incident flux densities are those which vary with time. For the static parameters, as usual, we introduced a specific variation around their reference value: $\beta = \beta^{ref}(1+K)$. For the time-dependent parameters, we performed two analyses. The first one was according to $\beta(t) = \beta^{ref}(t)(1+K)$ (labeled as

"systematic" in figure 7). For the second one (labeled as "stochastic" in figure 7), we added random variations to the nominal time evolution as observed over a period of two days. We applied a uniform centered distribution according to:

$$\beta(t) = \beta^{ref}(t) + \overline{\beta^{ref}} K(2u_{0,1} - 1)$$

(9)

with $K = \Delta\beta(t) / \overline{\beta^{ref}(t)} = cst$ and $u_{0,1}$ is the uniform distribution on the support [0,1] ; $\overline{\beta^{ref}(t)}$ in Kelvin if β is the air temperature. In both cases of systematic deviation of the parameter, the reduced sensibility is approximated by the finite difference:

$$S_i = \left(T_{\beta_i + \Delta\beta_i} - T_{\beta_i}\right) / K$$

(10)

For the second analysis of the time-dependent parameters, series of simulations have to be performed with different random drawings. At each time, the temperature scatter is then compared with the nominal temperature at this time. The reduced sensibility is then given by the ratio of the standard deviation of the simulated temperature with respect to the reference temperature, over the standard deviation of the uniform distribution of the considered parameter:

$$S_i(t) = \sigma_T^*(t)\sqrt{3} / K$$

(11)

We plotted the reduced sensitivity to the thermal parameters (effusivity and square root of diffusion time) of the three layers of the wall in figure 5. For instance, a reduced sensitivity of 1°C means that a deviation of 10% on a parameter implies a deviation of 0.1°C on front temperature. We can see that the parameters of the third layer have less influence on the temperature than the first layer and the insulating layer. The sensitivities of this two first layer are inferior to 3°C. Maximum absolute values of sensitivity are those with respect to the front layer effusivity; it is negative at day and positive at night.
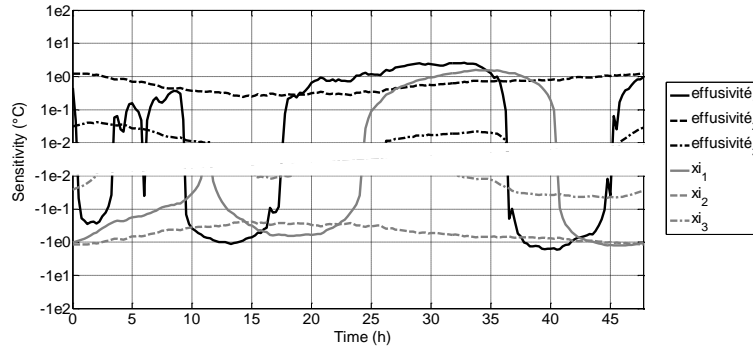
Fig. 6. Relative sensitivity of thermal properties of the three-layer wall

The optical parameters and the incident flux densities describe the radiative front excitation. In figure 6 we plotted the absolute values of the reduced sensitivity; it is actually negative for the albedo. The ratio between the sensitivities to albedo and to the VNIR flux varies from 5 to 12. This ratio should be about 3.6 when taking into account the actual value of the albedo. We observe a higher value because the sensitivity to VNIR variations as obtained through Eq. (9) is lower than the one obtained when considering a *systematic* VNIR relative variation. This deviation is due to the inertial effect of the wall: for the radiative flux, which is randomly scattered at high frequency about the reference values, the front temperature is less influenced than with a uniform deviation of the radiative flux which obviously has the same consequence that as an absorptivity variation.
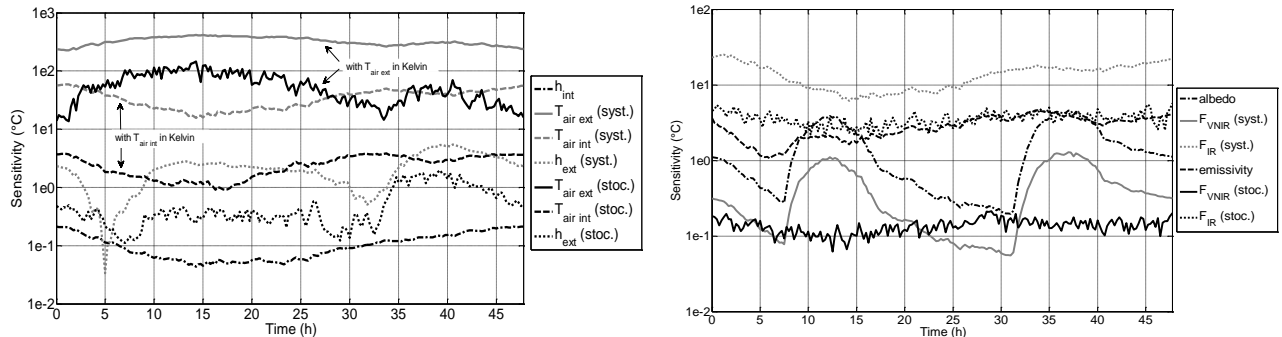
Fig. 7. Relative sensitivity of convective (a) (at left) and radiative (b) (at right) parameters

We can see on figure 7.a the sensitivity of the front temperature to the convective coefficients and to the external and indoor air temperature. Overall, the front temperature has a low sensitivity to the indoor parameters. The external parameters and a systematic error on indoor temperature are most critical to the results. For instance, during the two days presented here, the sensitivity to the air temperature reaches about 300°C for the systematic variation analysis,

respectively 100°C for the stochastic analysis. It means that an error of 0.5% on the air temperature (in Kelvin), i.e. an error of around 1.4°C, then implies an uncertainty of around 1.5°C, resp. 0.5°C, on the front surface temperature.

The front temperature is more sensitive to thermal and geometrical parameters of first two layers, to the outdoor convective parameters and to the IR radiation and emissivity. Therefore these parameters have to be measured with a high accuracy: the uncertainty has to be lower than about 5%, or 0.17% for air temperature (in Kelvin), to get an error lower than 0.5°C. Furthermore indoor parameters would be extremely difficult to evaluate from external surface temperature through data inversion.

4. Experimental

4.1. Description

The experimental measurement campaign BATIR took place in winter 2013 on the military airbase 701 at Salon-de-Provence, France. The thermal behaviour of two buildings was studied for a period of two weeks (see figure 7). Two meteorological stations were used: one station (Campbell CR23X) was placed in an open area next to the runway and the other one (Campbell CR3000) was placed between the two buildings. Meteorological data were collected in order to estimate outdoor air temperature, wind velocity, global solar irradiance and IR irradiance. Air temperature inside the rooms was measured by probes suspended close to back side of the facade of interest (EL-USB-1-PRO). The spectral reflectance of the participating surfaces was measured with a spectroreflectometer, in the [0.4-2.5 µm] domain (ASD) and in the [2.9-13.3 µm] domain (SOC400T). The thermography analysis was realised during two separate periods of 24 hours. Two 512x640 IR cameras were used: a band II camera (FLIR SC6000) and a band III camera (FLIR SC7000). The latter camera has been provided with a narrow filter. The half-height spectral bands are respectively [3-5 µm] and [8.4-8.7 µm]. The cameras were periodically aimed at an extended blackbody for drift correction and for establishing a relation between output signal and IR radiance in the respective bandwidths. The first 24h thermographic measurement was performed by aiming the south façade of building LC3 from the north façade of building LC4. For the second 24h thermographic measurement we performed the opposite. During the second thermographic measurement, five thermocouples and a fluxmeter were fixed on the north façade of building LC4 for independent values of the temperature and the heat flux at six particular locations of the wall. Thermography was also performed with a microbolometer camera onboard of a motor glider. The camera was flown at about 40 m.s^{-1} and about 400 m altitude. It was aiming at nadir. During the first thermography period, two flights were performed short after sunrise, at midday, and during the second period, three flights were performed short after sunrise, at midday and shortly before sunset.
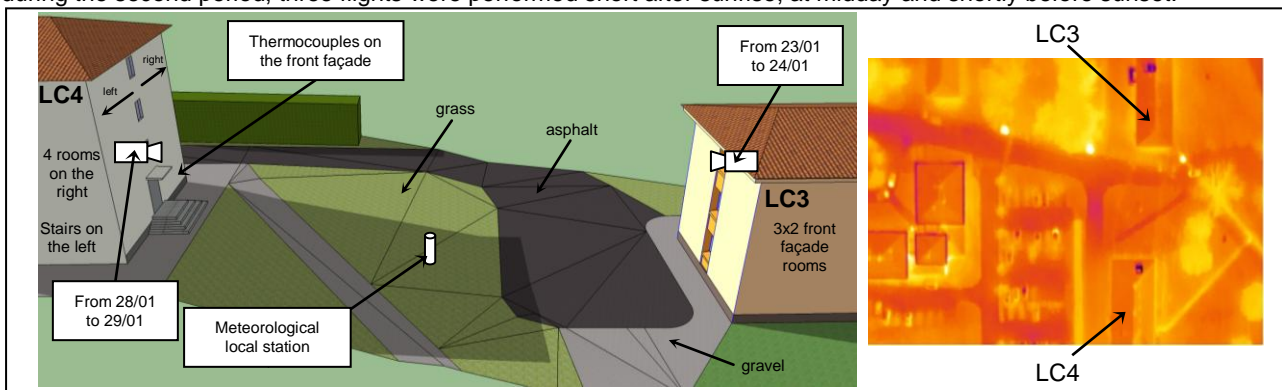
Fig. 8. Analysed scene during BATIR campaign (at left) and airborne IR image (at right)

4.2. Experimental validation of SUSHI

The first experimental validation consisted in comparing our thermal model results with the thermocouple measurements on the north facade of the building LC4. The wall is made of three layers, consisting of a reinforced concrete layer, an isolating PS layer and a BA13 plaster board. The respective layer thicknesses and thermal properties, as obtained from literature are given in table 2. The outside convective coefficient was calculated from wind speed by the empirical formula, with wind speed measured at the building level. Wind speed data were available from two meteorological stations, one in an open area, and the other between the buildings. The first data series was available for whole month and the second one only for the last day of interest (started at 10:00). One day of data was thus missing for allowing the 48h analysis as described in § 2.2.1. Data from the first station were thus used for the missing day by applying a correction factor that was established by comparing the wind data recorded during the second, i.e. common day. This extrapolation is justified by the fact that the wind direction didn't change during this couple of days. The outside air temperature was given by the first station. The inside convective coefficient was arbitrarily fixed to 10 W.m^{-2}.K^{-1}, with air temperature measured at an approximate distance of 5 cm from the surface. The albedos were calculated from the measured spectral reflectance by weighting them with the solar spectral radiation provided by the atmosphere radiative transfer model MATISSE. The average emissivities were calculated from the IR measured reflectance by weighting them with the Planck's law corresponding to a surface at 5°C. The MATLAB version of the program was used here again, with

boundary conditions fixed from 3D computations by SOLENE and SUSHI. Let us mention here that the net radiative infrared flux was obtained from the temperature 3D field estimated by the SOLENE thermal core; only the first group of iterations aimed at updating the convective heat flux term was thus performed; there was no updating of the radiative infrared flux term (see figure 9). Temperature measured with a given thermocouple is compared with the simulated temperature of the corresponding facet. These thermograms are shown in figure 9.
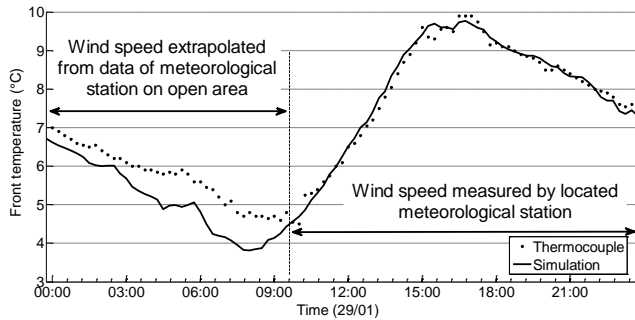
Fig. 9. *Comparison between temperature simulated by SUSHI and measured by thermocouple*

Table 2. Description of wall					
Thickness and thermal properties					
Layer	e (m)	k (W.m^{-1}.K^{-1})	$\rho.C_p$ (J.m^{-3}.K^{-1})	b (J.s$^{-1/2}$.m^{-2}.K^{-1})	ξ (s$^{1/2}$)
Reinforced concrete	0.17	1.8	2.112e6	1950	184.1
PSE	0.027	0.035	31.26e3	33.1	25.5
Plaster (BA13)	0.013	1.0	1.44e6	1200	15.6

4.3. Experimental validation of the full chain of simulation
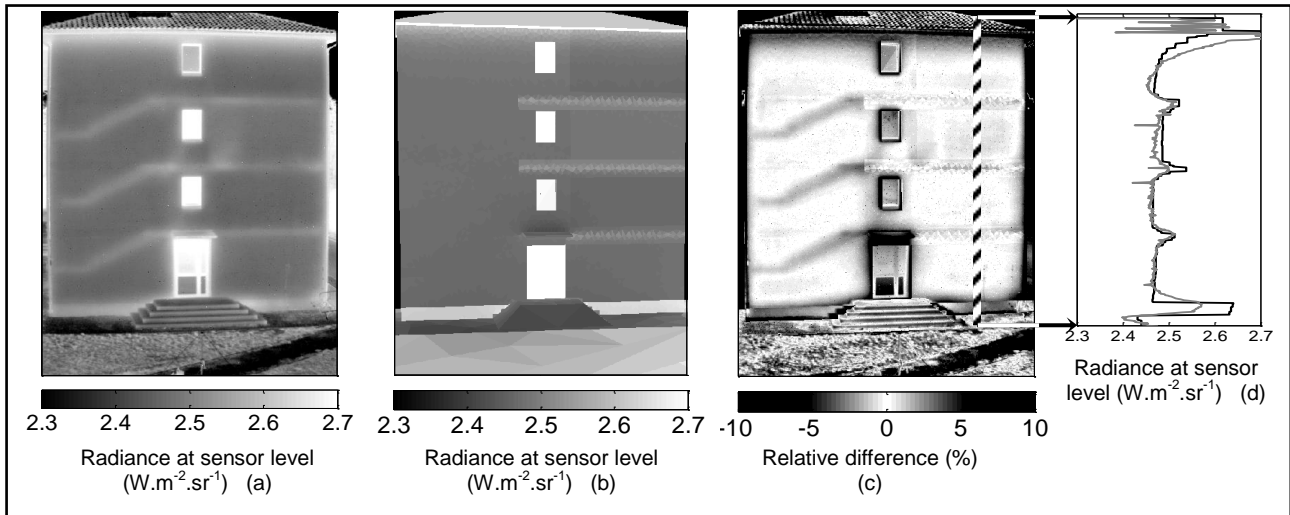
Fig. 10. *Comparison between radiance simulated by SOLENE/SUSHI/MOHICANS and measured by thermography*

The façade of the building called "LC4" is used for the validation of the full chain of programs. The figure 10 presents three images of this façade: (a) is the infrared image measured by the camera SC7000 (in the [8.4-8.7 μm] spectral band), (b) is the simulated image obtained at the outlet of the chain, (c) is the relative difference between the real and the simulated image and (d) is the vertical profile of radiance along the right side of the façade.

These images were recorded at 05:00 PM on January 29th. Two days were used to take into account the thermal dynamic of the scene. The scene was triangulated with 9975 facets. Areas with known thermal bridges (and visible on the IR images) were meshed more densely. For convenience, grounds, stairs, roof, windows and the door contained few facets (and the steps of the stair wasn't modelled). At the moment, half-transparency materials aren't processed by the programs; this is why temperatures and radiances of windows aren't realistic. 2D thermal bridges induced by floors were taken into account by the simulation but not the thermal bridges induced by indoor stairs (on the left of the façade) and the 3D areas induced by the floors near the right corner. The image of the relative difference shows that the radiances of 1D-wall parts are correctly estimated with a relative difference less than 2.5%. Heat losses induced by the thermal bridges at floor junctions are relatively well retrieved by the simulation despite the size of the facets used here. Differences observed on the ground and the roof are explained the significant roughness of these surfaces (they were considered flat in the 3D model). The difference reaches 9% at the soffit (the underside of the roof): the radiance of this part is higher than revealed by the simulation because the internal temperature can be higher than the measured temperature and the material is unknown. From this part some warm air could flow from the attic against the façade, which explains the difference on the top of the 3rd floor.

5. Conclusion

In this work a numerical tool was developed for the simulation of the temperature field and the infrared rendering in an urban scene. The radiation energy budget at each facet of the modelled environment takes into account the multiples reflections of the incident solar flux (by SOLENE) and the IR radiative coupling between facets (by the new code SUSHI). The 1D response factors are calculated interactively by the quadrupole method whereas the 2D response factors are extracted form a database that was built from finite element calculation results. Computed results show that two days are necessary for catching the thermal evolution of a typical wall at 0.1°C precision though our periodic approach (the error is about 0.2°C for soils). The sensitivity study indicates the significance of thermal properties of the first two layers of a wall, and the influence of measurement errors about external air temperature, emissivity and infrared incident flux. Validations of this tool were performed by thermocouples and infrared thermography, with data acquired during the experimental campaign BATIR. Final results show little difference between measured and simulated radiance for the wall and the considered thermal bridges. Higher differences are observed for the roof (because the geometry of tiles) and the ground (because of its roughness) and at some locations for which boundary conditions were not well known (soffit and crawl space level). Further studies will be performed for analysing the airborne data.

6. Acknowledgements

REFERENCES

[1] Masson V., "A physically-based scheme for the urban energy balance in atmospheric models". Bound.-Layer Meteor. vol. 94, pp. 357-397, 2000.

[2] De la Flor F.S., Dominguez S.A., "Modelling microclimate in urban environments and assessing its influence on the performance of surrounding buildings". Energy and Buildings, vol. 36, pp. 403-413, 2004.

[3] Kanda M., Kawai T., Kanega M., Moriwaki R., Narita K., Hagishima A., "A simple energy balance model for regular building arrays". Boundary-Layer Meteorology, vol. 116, pp. 432-443, 2005a.

[4] Kastendeuch P.P., Najjar G., "Simulation and validation of radiative transfers in urbanized areas". Solar Energy, vol. 83, 2009.

[5] Asawa T., Hoyano A., Nakaohkubo K., "Thermal design tool outdoor spaces based on heat balance simulation using a 3D-CAD system". Building and Environment, vol. 43, pp.2112-2123, 2008.

[6] Krayenhoff E. S., Voogt J. A., "A microscale three-dimensional urban energy balance model for studying surface temperatures". Boundary-Layer Meteor., vol. 123, pp. 433-461, 2007.

[7] Dupont S., Mestayer P.G., "Parameterization of the urban energy budget with the submesoscale soil model". Journal of Applied Meteorology and Climatology, vol. 45, pp. 1744-1765, 2006.

[8] Yang X., Li Y., "Development of a 3D urban energy model for predicting and understanding surface temperature distribution". Boundary-Layer Meteorology, vol. 149, pp. 303-321, 2013.

[9] Groleau D., Fragnaud F., Rosant J. M., "Simulation of the radiative behavior of an urban quarter of Marseille with the SOLENE model". International Association for Urban Climate, pp. 335-338, 2003.

[10] Hénon A., Mestayer P.G., Groleau D., Voogt J., "High resolution thermo-radiative modeling of an urban fragment in Marseilles city center during the UBL-ESCOMPTE campaign". Building and Environment, vol. 46, pp. 1747-1764, 2011.

[11] Idczak M., Groleau D., Mestayer P., Rosant J.-M., Sini J.-F., "An application of the thermo-radiative model SOLENE for the evaluation of street canyon energy balance". Building and Environment, vol. 45, pp. 1262-1275, 2010.

[12] Wang S., Chen Y., "Transient heat flow calculation for multilayer constructions using a frequency-domain regression method". Building and Environment, vol 38, pp.45-61, 2003.

[13] Stephenson D.G., Mitalas G.P., "Calculation of heat conduction transfer functions for multilayer slabs". ASHRAE Transactions, vol. 77, pp. 117-126, 1971.

[14] Gastellu-Etchegorry J.P., Grau E., Lauret N., "A 3d model for remote sensing images and radiative budget of earth surfaces". Modeling and Simulation in Engineering, edited by Prof. Catalin Alexandru, 2012.

[15] Fontanilles G., Briottet X., Fabre S., Trémas T., "Thermal infrared radiance simulation with aggregation modeling TITAN an infrared radiative transfer model for heterogeneous 3D surface - application over urban areas". Appl. Opt., vol. 47, no 31, 2008.

[16] Labarre L., Caillault K., Fauqueux S., Malherbe C., Roblin A., Rosier B., Simoneau P., "An overview of MATISSE-v2.0". Remote Sensing, vol. 782802, 2010.

[17] Perez R., Seals R., Michalsky J., "All weather model for sky luminance distribution_Preliminary configuration and validation". Solar Energy, vol. 50, No. 3, pp. 235-245, 1993.

[18] Cohen M. F., Chen S. E., Wallace J. R., Greenberg D. P., "A progressive refinement approach to fast radiosity image generation". Computer Graphics, vol. 22, No. 4, 1988.

[19] Pailhes J., Pradere C., Battaglia J.-L., Toutain J., Kusiak A., Aregba A.W., Batsale J.-C., "Thermal quadrupole method with internal heat sources". International Journal of Thermal Sciences, vol. 53, pp. 49-55, 2012.

[20] Frigo M., Johnson S., www.fftw.org.

[21] Maillet, D. et al. "Thermal quadrupoles: solving the heat equation through integral transforms". John Wiley & Sons Inc, 2000.

[22] Thomas C., Doz S., Briottet X., Lachérade S., "AMARTISv2: 3D radiative transfer code in the [0.4; 2.5 µm] spectral domain dedicated to urban areas". Remote Sensing, vol. 3, pp. 1914-1942, 2011.

[23] Bouyer J., "Modélisation et simulation des microclimats urbains Étude de l'impact de l'aménagement urbain sur les consommations énergétiques des bâtiments". Ph. D. Thesis, 2009.

[24] Krapez J.-C., Tadé, V., Barillot P., Miesch C., Modélisation analytique de la variabilité spatiale et temporelle de la température de sols nus naturels, Congrès SFT 2004 Presqu'île de Giens (France).